Supplementary Information

Inverse melting and re-entrant transformations of the vortex lattice in amorphous Re_6Zr thin film

Rishabh Duhan[*], Subhamita Sengupta[*], John Jesudasan, Somak Basistha and Pratap Raychaudhuri[1]

Tata Institute of Fundamental Research, Homi Bhabha Rd, Mumbai 400005, India.

I. Filtering $G(\boldsymbol{r}, V^{coh})$ maps

Filtering of $G(\boldsymbol{r}, V^{coh})$ maps is done to remove the noise in the image. Figure 1S(a) shows a representative raw image. We first perform 2D Fast Fourier Transform (FFT) of this image (Fig. 1S(b)). The FFT shows diffused Bragg spots corresponding to the disordered vortex lattice, along with a diffuse background at higher $\boldsymbol{q}$-values corresponding to high frequency noise. To remove the noise, we suppress this intensity at high $\boldsymbol{q}$ values as shown in Fig. 1S(c). We then take Inverse FFT to get filtered image (Fig. 1S(d)).

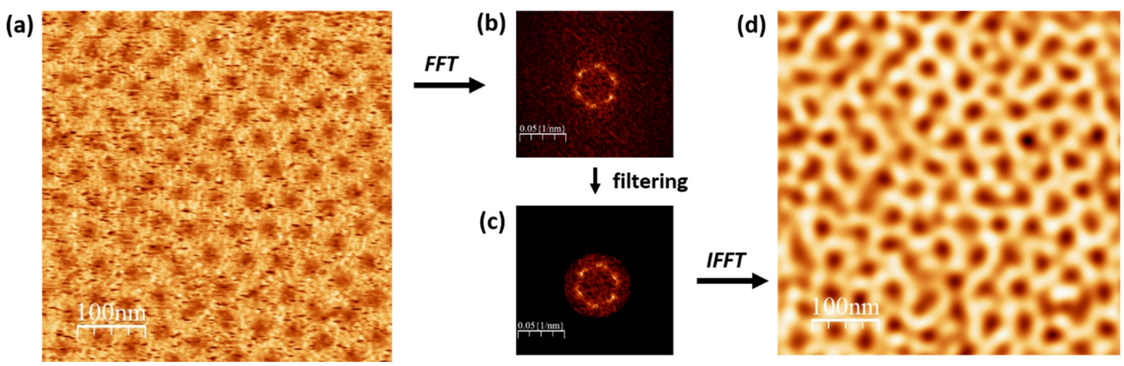

Fig. 1S (a) A raw image taken using STS. (b) 2D FFT of image. (c) Filtered FFT by suppressing high frequency noise. (d) Filtered image obtained by taking IFFT of (c).

II. Pinned vortex liquid at 1 kOe, 460 mK

At 460 mK we observe the inhomogeneous VL at 1 kOe. Fig. 2S (a)-(d) shows four $G_N(\boldsymbol{r})$ maps taken consecutively over the same area. Since the vortex density is low we captured these images over a larger area, i.e. 800 nm × 800 nm, to have sufficient number of vortices within the field of view. Consequently, each of these images were captured over 24 min. We observe well resolved minima in each image. Here, since the distance between minima is large, we do not observe any complete hop of vortices from one minimum to another. However, the position of some minima changes due to incomplete hops. Fig. 2S(e) shows positions of minima obtained from all 4 images alongside with motion path connecting them.

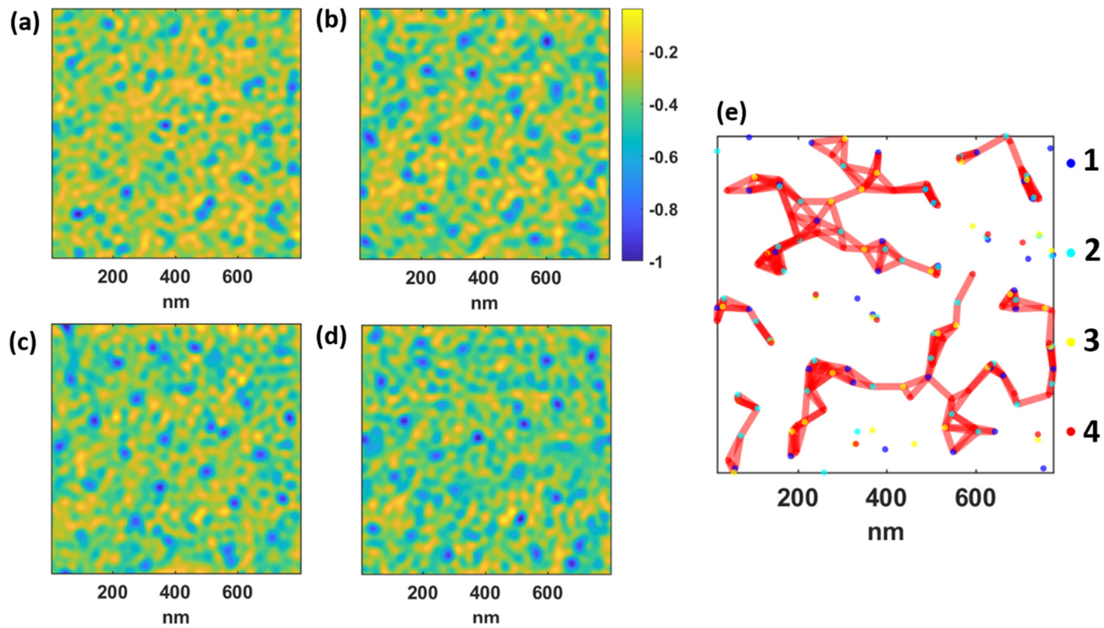

Fig. 2S (a)-(d) $G_N(\boldsymbol{r})$ maps taken at 1 kOe and 460 mK. (e) Position of $G_N(\boldsymbol{r})$ minima for four consecutive images along with motion path of vortices.

III. Re-entrant behavior of VL at 2K

The re-entrant transformation of vortex state is also observed at 2 K. Fig. 3S(a) shows formation of inhomogeneous liquid at 3 kOe along with the global motion path of vortices. As we increase the field, we can see vortex state getting more ordered along with decrease in motion till 20 kOe (Fig. 3S(b)-(c)). At 30 kOe, it again forms an inhomogeneous liquid state (Fig. 3S(d)). Same can be seen in Fig. 3S(e) where Ψ_6 peaks and f_G shows a minimum at 20 kOe.

IV. Determination of critical current, I_c

Pulsed *I-V*, with a rectangular pulse of width 50 ms and interval of 6 s respectively, is taken to avoid heating at high current. Fig, 4S(a) shows pulsed I-V curves for 5 kOe, 15 kOe and 30 kOe at 460 mK. Zoomed in I-V curves for various magnetic fields at 460 mK is shown in Fig. 4S(b) .

Usually, with increase in applied current, the vortex state eventually goes to Bardeen Stephen flux flow state which is characterized by flux flow resistance $R_{ff} = R_N(\frac{H}{H_{c2}})$, where R_N is normal state resistance. Thus, we get a linear region in *I-V* curves from where we extrapolate to obtain I_c from the intercept on current axis. However, in thin films, formation of inhomogeneous vortex state complicates the scenario, and one does not get a clear linear region in *I-V* characteristics (See ref. 5). Instead, there is a rounding off of the *I-V* curves due to vortex creep which extends till depairing current is reached (Fig. 4S(a)). Therefore, here we use a simpler criterion to determine I_c, namely, the current at which the voltage reaches 30 μV. Fig.

4(b) shows zoomed in I-V curves for various magnetic fields. Value of current where the horizontal dashed line at 30 μV intersects the *I-V* curves marks the criterion for determining critical current (Fig. 4S(b)).

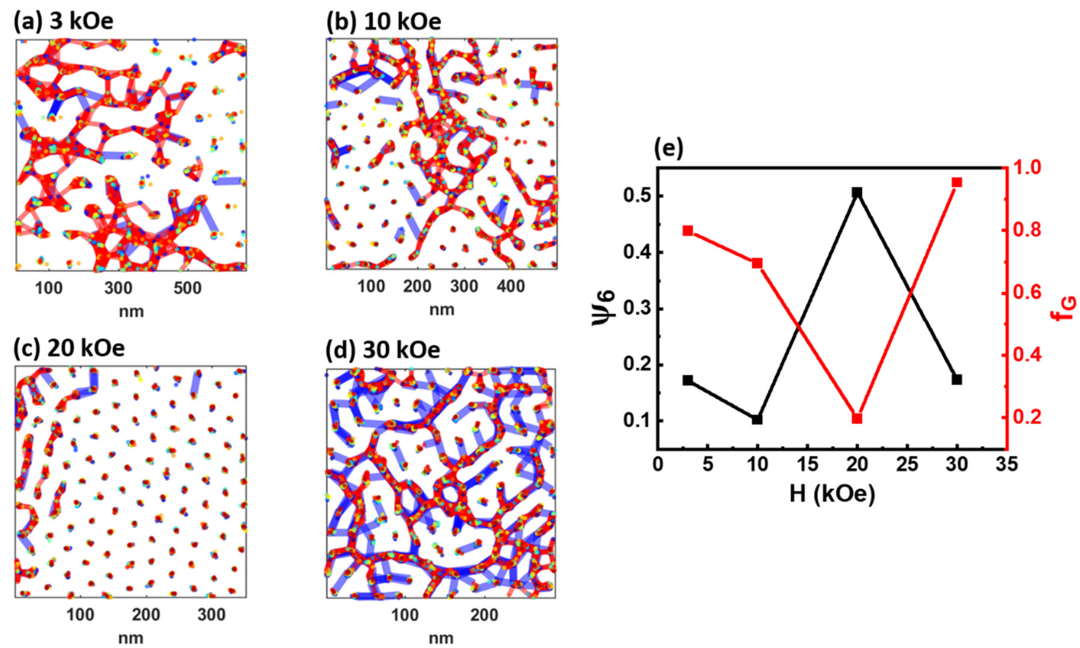

Fig. 3S (a)-(d) Evolution of global motion path of vortices with magnetic field at 2 K. (e) Variation of corresponding Ψ_6 and f_G with magnetic field at 2 K.

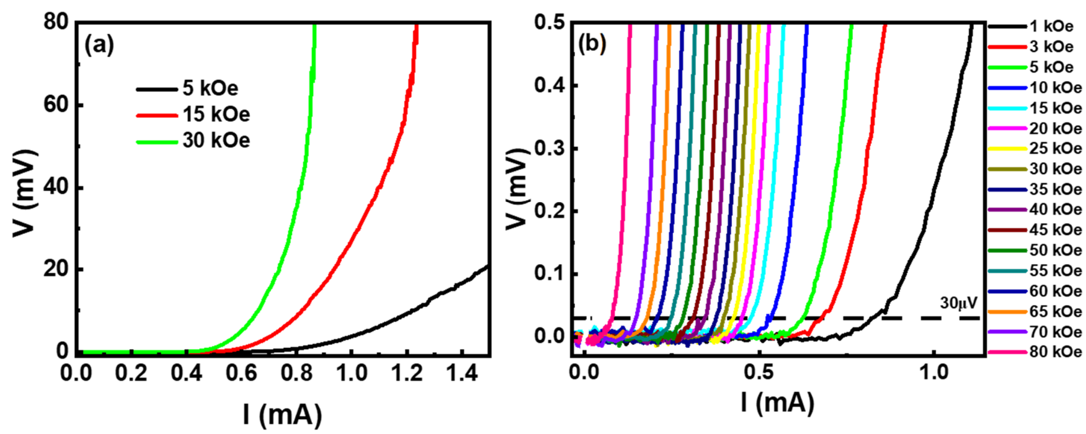

Fig. 4S (a) Pulsed *I-V* curves for 5 kOe, 15 kOe and 30 kOe respectively taken at 460 mK. (b) Zoomed in *I-V* curves for various magnetic fields at 460 mK. Horizontal dashed line is draw at V = 30 μV. I_c at a field is determined from the value of I where the horizontal dashed line intersects with the respective *I-V* curve.

V. Comparison of pinning strength

In terms of pinning the 20 nm *a*-ReZr film used in this study is intermediate between the very weakly pinned 20 nm thick *a*-MoGe film reported in ref. 20 and the strongly pinned 5 nm *a*-ReZr film used in ref. 5. To compare the pinning strength of these films we plot $J_c - H$ at 460 mK for these 3 films using the same criterion described in Section IV (Fig. 5S). Since collective effects are small at low fields, the low-field J_c value is a good indicator of pinning strength. We observe that below 40 kOe, J_c for the 20 nm *a*-ReZr film used here is indeed larger than the 20 nm thick *a*-MoGe film but smaller than the 5 nm *a*-ReZr film.

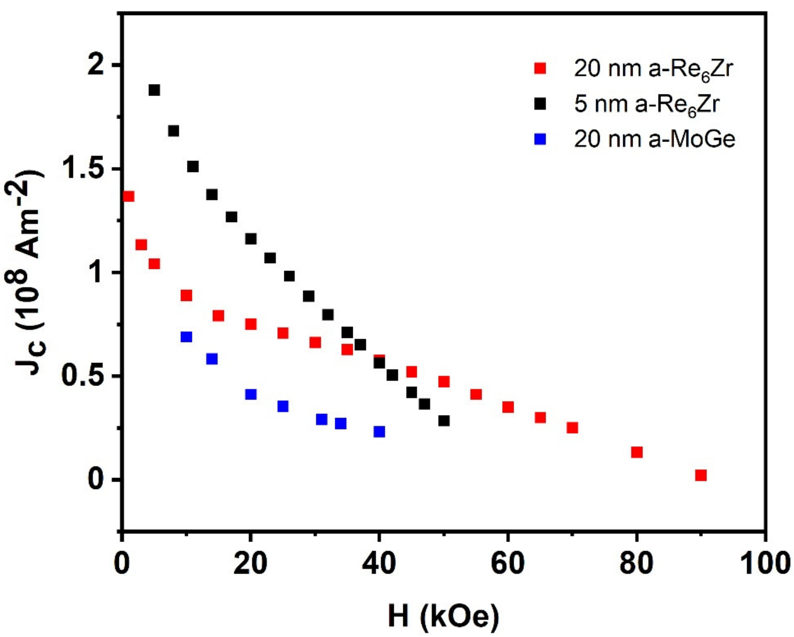

Fig. 5S. Variation of critical current density J_c with magnetic field for 5 nm thick *a*-ReZr, 20 nm thick *a*-ReZr and 20 nm thick *a*-MoGe thin films respectively.

VI. Signature of reentrant transition in the thermal activation barrier for vortices, *U*

In the main paper we have shown signature of the re-entrant transition in the magnetic field variation of J_c. Here we show that similar signature is also seen in effective pinning barrier, *U*, for thermally activated motion for vortices.

To determine *U,* in Fig. 6S(a) we plot the logarithm of the resistance resistance in ohms, ln(*R*), as a function of 1/*T*. At low temperatures the resistance follows a simple activated behaviour, $R = R_0 e^{-U(H)/kT}$ (where *k* is the Boltzmann constant). In Fig. 6S(b) we plot *U,* (extracted from the slope of $ln(R)$ vs $\frac{1}{T}$) as a function of H in semi-log scale. We observe that for $H \leq 5\ kOe$ and $H \geq 40\ kOe$, the data fall on a straight line such that the magnetic field variation is described by a single functional form, $U(H) = U_0 ln(H_0/H)$ where $H_0 = 90.3\ kOe \sim H_{c2}$. This

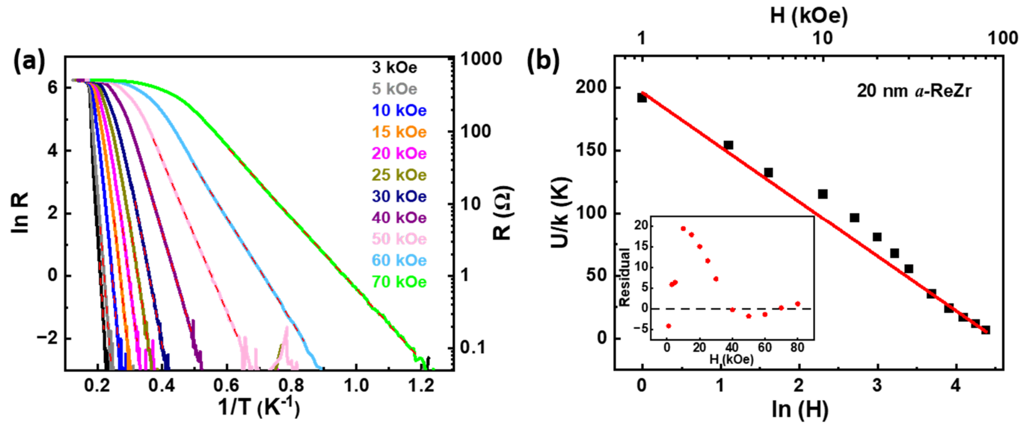

Fig. 6S. (a) Resistance versus temperature for the 20 nm thick a-ReZr film plotted as ln(R) (R in Ohms) versus 1/T; the dashed line are linear fits to these curves showing that the variation at low temperature follows a simple activated behavior. U is extracted from the linear slope of the fit. The right axis shows the resistance in log-scale. (b) Variation of U with ln(H) (H in kOe). The red line is a fit to, $U(H) = U_0 ln(H_0/H)$, for the data in the range $H \leq 5\ kOe$ and $H \geq 40\ kOe$. The inset shows the difference between the data and the fit.

functional form is observed in many thin films and is expected when transport is dominated by thermal activation of dislocation pairs. On the other hand, in the magnetic field range $5\ kOe < H < 40\ kOe$, where the vortex lattice gradually gets ordered, U is larger than what is expected from this curve. This increase results from the increase in the shear modulus (C_{66}) as the vortex lattice gets ordered which makes the formation of dislocation pairs more expensive (see ref. 25). In contrast for 5 nm a-ReZr thin film investigated in ref. 5 where vortices form an inhomogeneous liquid over the entire range of magnetic field, the functional form $U(H) = U_0 ln(H_0/H)$ captures the variation of U over the entire magnetic field range (See Fig. 1(a) of Ref. 5).